# Mechanism behind dry etching of Si assisted by pulsed visible laser

Jason A. Peck, and David N. Ruzic

Citation: Journal of Applied Physics **122**, 173304 (2017); doi: 10.1063/1.4991886
View online: https://doi.org/10.1063/1.4991886
View Table of Contents: http://aip.scitation.org/toc/jap/122/17
Published by the American Institute of Physics

**Articles you may be interested in**

Ultraviolet out-of-band radiation studies in laser tin plasma sources
Journal of Applied Physics **122**, 173303 (2017); 10.1063/1.4986782

Energy distributions of electrons emitted by a biased laser-produced plasma at $10^{13}$ W cm$^{-2}$
Journal of Applied Physics **122**, 173302 (2017); 10.1063/1.4997708

Secondary electron emission yield from high aspect ratio carbon velvet surfaces
Journal of Applied Physics **122**, 173301 (2017); 10.1063/1.4993979

Standoff high energy laser induced oxidation spectroscopy (HELIOS)
Journal of Applied Physics **122**, 173102 (2017); 10.1063/1.4999918

Actuation of a lean-premixed flame by diffuse non-equilibrium nanosecond-pulsed plasma at atmospheric pressure
Journal of Applied Physics **122**, 173305 (2017); 10.1063/1.4995964

Thermoelectric band engineering: The role of carrier scattering
Journal of Applied Physics **122**, 175102 (2017); 10.1063/1.4994696

AIP | Journal of Applied Physics SPECIAL TOPICS

JOURNAL OF APPLIED PHYSICS **122**, 173304 (2017)

# Mechanism behind dry etching of Si assisted by pulsed visible laser

Jason A. Peck and David N. Ruzic[a)]
*University of Illinois Urbana-Champaign, Department of Nuclear, Plasma, and Radiological Engineering, 104 S. Wright St., Urbana, Illinois 61801, USA*

(Received 23 June 2017; accepted 6 October 2017; published online 2 November 2017)

Poly-Si films were etched using a 13.56 MHz capacitively coupled plasma source while simultaneously being exposed to a pulsed Nd:YAG laser using 266 and 532 nm lines, with Gaussian pulse durations of 100 Hz and 7 ns. For a fluorocarbon etch recipe of 50:8 sccm Ar:$C_4F_8$ with varying $O_2$, a minimum laser intensity for the etch onset was necessary to overcome $CF_x$ polymer deposition. This etch onset occurred at $6 \pm 1$ mJ/cm$^2$/pulse; beyond this onset, the etch rate increased linearly with laser intensity. Null results of laser etch enhancement using continuous wave diode sources demonstrated the necessity of the instantaneous application of the pulsed Nd:YAG source. To determine the mechanism of laser etch enhancement at 532 nm, highly doped Si samples were tested, with varying optical absorption depths while keeping the photon energy constant. It was shown that at phosphorus contents of $10^{19}$ cm$^{-3}$ and $10^{21}$ cm$^{-3}$, 532 nm etch enhancement trends were 1.7× and 3.7× higher than those on intrinsic Si, showing that instantaneous surface heating was key in desorbing involatile etch products. Further investigation of the surface fluorine content via X-ray photon spectroscopy showed that distinct desorption stages occurred for increasing pulse energy—trends which aligned very well with $SiF_x$ desorption promoted by steady-state wafer heating. Gas arrival/surface saturation experiments with varying pressures and pulse rates showed that, in straightforward etching discharges such as Ar/$SF_6$, laser removal per pulse plateaus when the pulse rate is lower than the rate of surface saturation, while in fluorocarbon-rich etch chemistries such as Ar/$C_4F_8$/$O_2$ mixtures, a minimum pulse rate must be maintained to overcome the $CF_x$ polymer layer being deposited. *Published by AIP Publishing.*
https://doi.org/10.1063/1.4991886

## I. INTRODUCTION

The manufacturing of integrated circuits (ICs) relies heavily on etching—removing materials on a wafer based on the stencil produced by lithography. As transistor features approach the 7 and 5 nm technology nodes following Moore's law,[1] surface fidelity becomes more and more important to the performance of the device. Current reliance on reactive ion etching (RIE) techniques may be detrimental to future devices due to induced damage by energetic ions.

This work explores a new process, combining the traditional etch plasma with light exposure of the wafer. Similar to ions, photons may be directed onto a target surface to etch anisotropically, but since photons carry negligible momentum, the induced disorder may be significantly reduced. This laser-assisted plasma etch process, dubbed Dry Etch Assisted by Laser (DEAL),[2] is presented as an alternative to reactive ion etching (RIE) for Si wafer processing in upcoming integrated circuit technology nodes.

Most research pertaining to photo-stimulated etching focuses on UV sources due to their high absorption in most materials. After all, Shin[3] demonstrated the role of etch product removal through the native VUV emission (Ar 104.8 and 106.6 nm lines) of the plasma itself. Some pursued Si etching under UV exposure in reactive ($Cl_2$)[4–6] and chemisorbed ($NF_3$ and $SF_6$)[7,8] gases, in wet etching conditions such as KOH,[9,10] and traditional plasma discharges of $CF_4/O_2$[11] or $Cl_2$/Ar.[12] Sesselmann[5] showed three distinct regions of photo-stimulated etching via UV (248 nm KrF and 308 nm XeCl), with material removal peaking at 0.01–0.03 Å/pulse and 400–600 mJ/cm$^2$/pulse intensity before transitioning into ablation. Maki and Ehrlich[13] showed an early form of atomic layer etching (ALE) through 193 nm ArF laser pulsing on GaAs in $Cl_2$, while Ishii[14] did the same with 248 nm KrF. Choy and Cheah[9] observed applications of surface structuring via the laser during wet etch to form porous silicon; on the other hand, Riedel[8] used 780 and 390 nm in $SF_6$ to texture Si into conical structures.

Out of the few that worked with visible light[5,7,14] (514.5 nm $Ar^+$ or frequency-doubled Yb), etch enhancement on Si was attributed to material heating. Holber[11] showed that continuous-wave (CW) $Ar^+$ 514.5 nm in $CF_4 + O_2$ could locally increase the etch rate significantly, but the energy demands to sustain a temperature gradient in Si were prohibitive.

Electron beams have also been used to selectively etch $SiO_2$ vs Si[15] not only at high temperatures but also at low temperatures in conjunction with $XeF_2$.[16] While these techniques share mechanisms of encouraging etch product removal, they are less compatible with modern 300+ mm single-wafer processing. A defocused low-power-density laser beam can traverse a plasma without interaction more easily than an electron beam.

Due to the age of most references, none pursued etching of smaller features (<100 nm), and damageless, room temperature etching was not a strong selling point for the

[a)]Author to whom correspondence should be addressed: druzic@illinois.edu

marginal improvements offered by introducing a light source at the time. This work seeks to revisit photo-assisted etching, addressing the potential of visible light to locally enhance or selectively etch materials under the requirements of IC manufacturing in the coming decade. Unlike UV irradiation, silicon oxide is transparent to visible light, while silicon is not, offering an important selectivity opportunity.

## II. EXPERIMENTAL APPARATUS

An etch testing laser and plasma in tandem were accomplished with a cylindrical capacitively coupled plasma (CCP) source, as seen in Fig. 1. The live electrode was driven at 13.56 MHz, matched with a high-low impedance L network, and cooled with deionized water through an electrically isolated back mount. This live electrode was recessed and enclosed in a cylindrical ground shield with a gap of ∼3 mm, enforcing a no-plasma condition following the projected breakdown voltage of argon at medium (10–40 mTorr) pressures according to Paschen's law.[17]

The light source primarily used was a Q-switched Nd:YAG system with a beam diameter of ∼8 mm and a maximum 100 Hz pulsing with a temporal Gaussian beam shape of 7 ns. Vibrational dithering of the optics was used to mitigate the effect of the laser speckle. The per-pulse power output was measured using a Spectra-Physics bolometer. Delivery of the laser to the sample was accomplished via a 5 mm hole in the ground electrode—large enough to expose a substantial area without disturbing the uniformity of the CCP discharge. This ground electrode was suspended by brackets mounted to the surrounding chamber (not pictured). A representation of the system is shown in Fig. 2.

Typical etch recipes involved a combination of $C_4F_8$ fluorocarbon etch gas, Ar buffer, and $O_2$ for polymer thinning or alternatively a simple $Ar/SF_6$ discharge. Fill pressures of 10–40 mTorr were used, moderated by 100 sccm Celerity Unit 1661 mass flow controllers and determined using a Pfeiffer capacitance manometer.

Laser irradiation is subject to non-linearities in the beam profile and causes speckles where some regions receive a significantly higher power. For the sake of processing uniformity and ellipsometric measurement of etch rates, a beam "dither" was added to spatially smooth the speckle. Commercially, this is often achieved by a vibrating

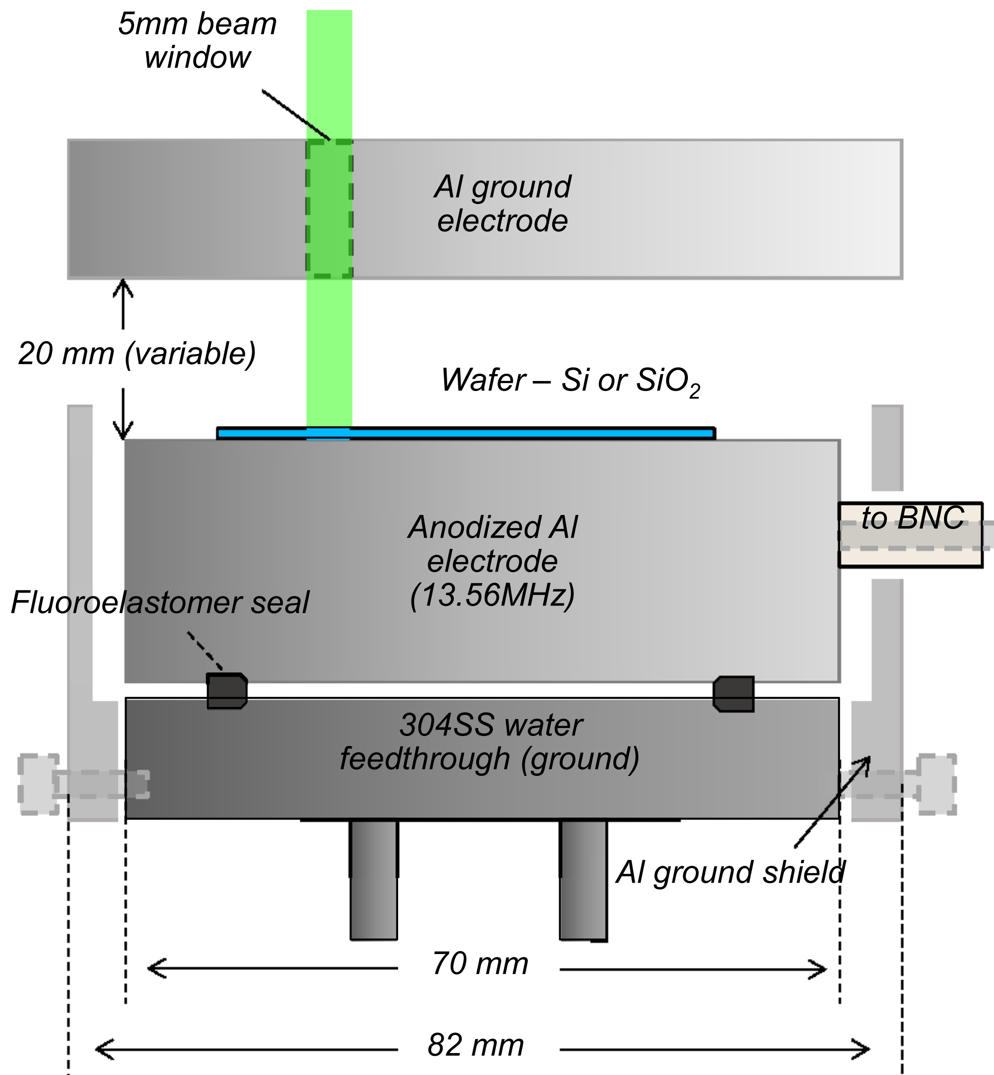


FIG. 1. Encapsulated RF-CCP design featuring a DI water-cooled substrate which doubles as a live RF electrode. The recessed electrode and ground shield design allows for plasma uniformity and optimal power delivery, while the 5 mm hole in the ground electrode provides a path for laser exposure.

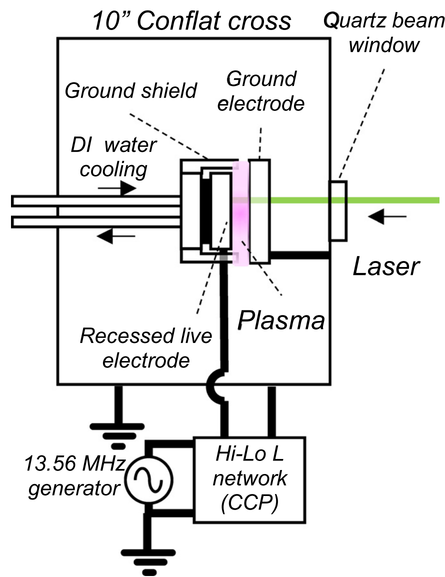


FIG. 2. Schematic of the Dry Etch Assisted by Laser (DEAL) vacuum chamber. Gases on the system included $C_4F_8$, $O_2$, $SF_6$, and Ar, and in later work, $CCl_4$ through a needle valve vapor draw system. The plasma source is pictured through the center viewport, with the hole in the live electrode (left) allowing the laser to reach the sample, mounted on the ground electrode (right, with the water cooling back-mount).

optic or target. To accomplish this, a motor with an off-axis weight was added to the optics column to introduce a dithering of the beam. While this method still leaves the mid-pulse speckle intact, as the pulse duration is ∼7 ns, the summation of multiple pulses that dithered a fraction of a millimeter across the substrate should represent a smoothed laser exposure profile. As seen in Fig. 3, the beam dithering was successful in smoothing the etch profile under the laser-exposed area. All experiments were conducted with the optics dithering in effect. The SEM also shows the effect of the etching on the surface after 5 min of 50:2 sccm Ar/$SF_6$ at 1.0 W/cm$^2$ RF–CCP discharge. The laser parameter was 532 nm at 40 mJ/cm$^2$ with 100 Hz and 7 ns pulse width.

For subsections C and D in Sec. III, the CCP source was replaced with an upstream ICP etcher with an independently biasable substrate in order to decouple ion energy and plasma density. (The details are given in Ref. 18.) Thus, etch radicals could be delivered with minimal ion bombardment to examine how the laser may be substituted for ions' directed sputtering effect.

## III. RESULTS AND DISCUSSION

### A. Etch enhancement with laser intensity

Starting with a fluorocarbon-saturated recipe of 50:8 sccm Ar/$C_4F_8$, the CCP discharge showed no etching and significant polymer growth. The introduction of the Nd:YAG laser during the discharge, however, resulted in the etch onset of poly-Si at roughly $6 \pm 1$ mJ/cm$^2$/pulse for both 266 and 532 nm. The etch rate increased moderately with increasing 532 nm pulse intensity, while 266 nm showed significant etch rate improvement (Fig. 4). In fact, the UV line achieved a 6–7× higher effect per unit intensity due to its higher photon energy.

Continuous wave (CW) diode laser sources of 405, 445, and 520 nm were similarly tested on poly-Si with the same recipe with no etch enhancement observed, even with intensities up to ∼200 W/cm$^2$. This null result insisted that despite the low average power of the Q-switched Nd:YAG, the high instantaneous power of its 7 ns pulses, on the order of 10s of MW/cm$^2$, was necessary in promoting etching.

800 nm thermal $SiO_2$ films were likewise tested for laser-assisted plasma etch, but no etch enhancement was seen even with 266 nm. The transparency of $SiO_2$ down to 200 nm was detrimental in affecting the exposed surface with the laser. It appears that the material's opacity to the chosen wavelength is key, with high intensity light being delivered to a small volume on the surface in poly-Si, rather than throughout the bulk in $SiO_2$. This trait of laser-assisted etching allows for a new form of etch selectivity. On top of relying on the chemical selectivity of the etched material, an optical selectivity is possible, activating etch on semiconductors over dielectrics using visible light or metals over semiconductors with infrared light.

### B. Doping variation at constant laser wavelength

To articulate whether the mechanism of etching at 532 nm was primarily thermal or photolytic, Si wafers of varying dopant levels were tested at varying absorption depths while maintaining a constant photon energy. Through doping, the concentration of free carriers was increased while leaving the etch/surface chemistry unchanged. The increase in the concentration of free carriers due to the presence of charge donors/acceptors is known to substantially increase absorption, particularly in the visible and infrared region. Dopant concentrations of $10^{19}$ and $10^{21}$ cm$^{-3}$ n-type (phosphorus) wafers were tested under the standard recipe

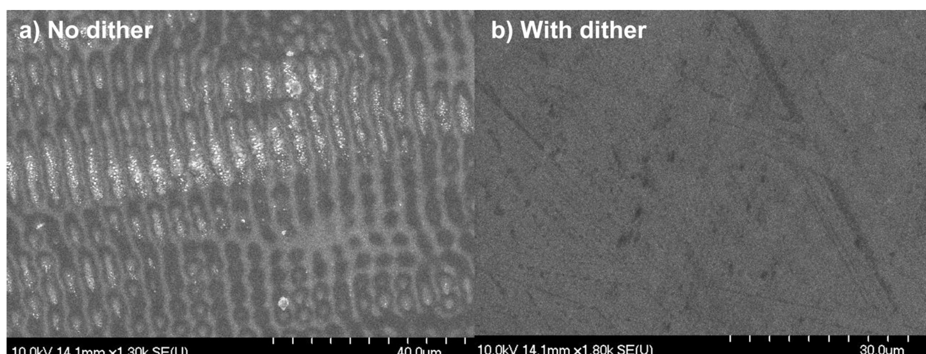


FIG. 3. Si wafer post-etch (see process conditions listed in the text) for (a) no dithering and (b) optics dithered via a 9VDC motor with the off-axis weight.

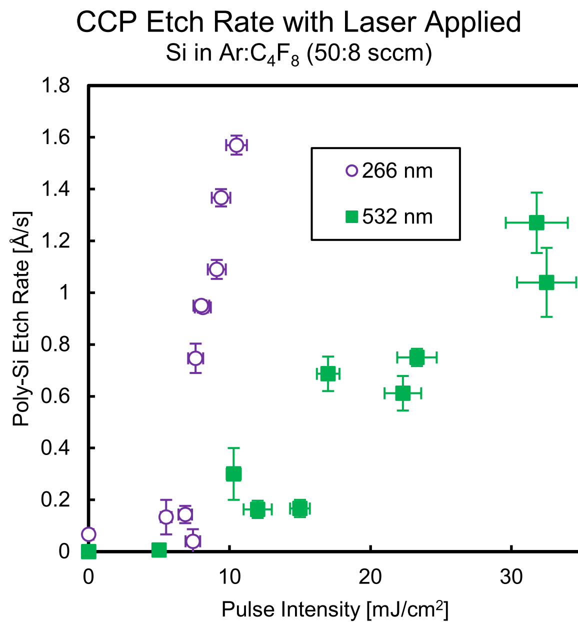


FIG. 4. Poly-Si etch rate data for a polymer-rich recipe of 50:8 sccm Ar/$C_4F_8$, with 100 Hz pulsed Nd:YAG laser exposure causing the etch onset at around 6 mJ/$cm^2$ for both 266 and 532 nm. Each data point is one sample.

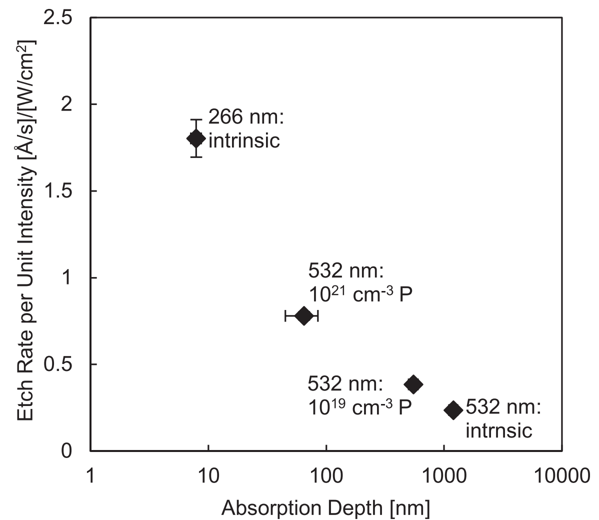


FIG. 6. The efficacy per unit intensity of laser etch enhancement is plotted against the penetration depth in Si. Values were obtained from the trend lines in Fig. 4. The use of highly doped Si has allowed the bridging of the gap between 532 and 266 nm. Absorption depths are predicted from the As-doped Si optical data in the study by Jellison *et al.*[19]

alongside intrinsic Si. From Jellison's measurements[19] of As-doped Si,[2] the expected absorption depths for 532 nm in Si at each of these conditions are 1100 ± 100 nm (intrinsic), 550 ± 100 nm ($10^{19}$ $cm^{-3}$ phosphorus), and 80 ± 20 nm ($10^{21}$ $cm^{-3}$ phosphorus).

The intensity trends caused by wafer doping are shown in Fig. 5. For dopant concentrations of $10^{19}$ and $10^{21}$ $cm^{-3}$, the etch rate showed scales 1.7× and 3.7× higher than intrinsic Si, respectively. Plotting the slope of etch rate vs. intensity, Fig. 6 shows a representation of how the laser's per-unit-intensity etch enhancement scales with the absorption depth at 532 nm. The fact that this value increases with the decreasing interaction volume for the same wavelength insists that at the lower photon energy of 2.33 eV, the mechanism is thermal desorption rather than the photolytic bond breaking typical of UV light.

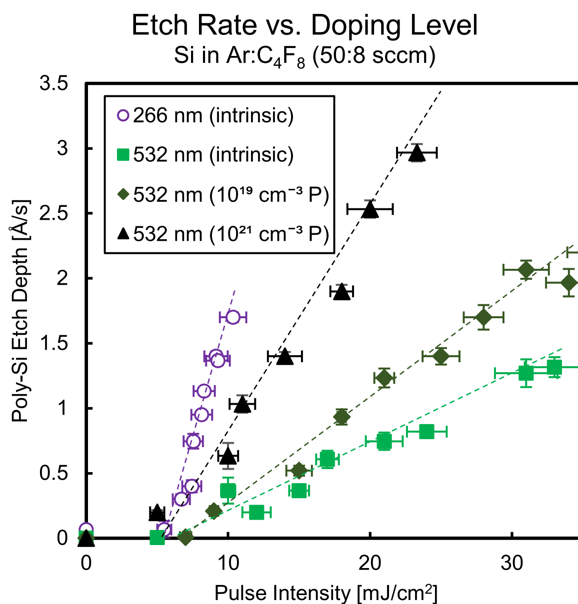


FIG. 5. Intensity ramping etch enhancement data for P-doped Si exposed to 532 nm Nd:YAG, contrasted against intrinsic Si at 532 and 266 nm. Average intensity may be determined by multiplying pulse intensity by the repetition rate (100 Hz). Each data point is one sample.

### C. XPS characterization of $SiF_x$ surface coverage

To further affirm the thermal aspect of the pulsed 532 nm laser's etch enhancement capability, X-ray photon spectroscopy (XPS) measurements of the etched Si surface post-laser exposure were taken and compared with the same spectra of Si post-etch under *in-situ* heating conditions in the XPS tool. If thermal desorption of involatile etch products was truly the dominant mechanism for etch enhancement at 532 nm, the F surface coverage of the $SiF_x$ surface vs. laser pulse intensity should compare well with un-exposed $SiF_x$ at steady-state heating conditions.

The XPS fluorine signal was expected to drop both when exposed to the pulsed laser and when heated through the substrate. Due to the significantly higher bond strengths of Si–F (565 kJ/mol) over F–F (155 kJ/mol) and Si–Si (222 kJ/mol),[20] this decrease in the F content was interpreted as desorption of $SiF_x$ etch products from the fluorinated Si surface. Similarly, Jeng's[21] work in rapid thermal processing of $F^+$-implanted Si shows that fluorine will reliably segregate to the surface, affirming that the drop in the surface F content measured by XPS is due to $SiF_x$ desorption, rather than F diffusing into the bulk wafer. Further corroborating this, desorption of $SiF_x$ at high temperatures was measured by Pullman[22] through residual gas analysis and calculated in MD simulations by Tinck.[23]

Two Si samples were prepared in a brief, no-bias Ar/$SF_6$ etch at room temperature. Once the etch was completed, one sample was exposed to a single Nd:YAG laser pulse with

varying intensities. The samples were then removed from vacuum, vented with $N_2$, and hermetically sealed for XPS surface characterization. In the XPS tool, the laser-exposed sample's spectrum was measured at room temperature, while the no-laser sample was heated *in-situ*. The resultant F surface coverage trends were then constructed, with maximums normalized to the room temperature, no-laser $F_{1s}$ peak intensity.

For both the single laser pulse samples and the no-laser samples heated in post, three distinct desorption stages were observed. For the single laser pulse case in Fig. 7, these stages occur at 40 ± 5, 90 ± 10, and 190 ± 10 mJ/cm$^2$/pulse, while the substrate heating case in Fig. 8 displays drops at 80 ± 10, 180 ± 10, and 400 ± 20 °C. It may be tempting to assign each successive desorption stage to $SiF_3$, $SiF_2$, and SiF according to the calculated physisorption energies in the study by Tinck.[23] To confidently do so, however, mass spectrometry would be necessary to characterize the desorbed surface species. Nonetheless, these data suggest that the DEAL process operates through $SiF_x$ desorption, increasing etch rates in the absence of ion bombardment.

In Fig. 9, the temperature for each desorption stage by substrate heating is compared against the simulated peak surface temperature for the corresponding laser intensities in Fig. 8. The peak surface temperature for laser-stimulated desorption is consistently higher than that of desorption by steady-state heating. This is likely due to the brief time (~100 ns) the $SiF_x$ surface spends at an elevated temperature before the energy delivered by the 7 ns pulse is dissipated into the bulk wafer.

### D. Gas arrival tests for $SF_6$ and $C_4F_8/O_2$ chemistries

The surface saturation time was of interest for a pulsed laser process based on releasing involatile etch products.

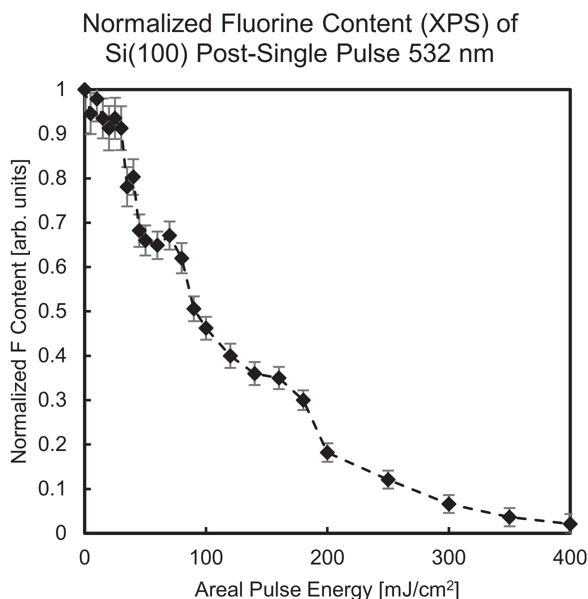


FIG. 7. Glancing angle XPS (75°) fluorine surface composition for Si(100) etched with low ion energy Ar/$SF_6$ plasma, then exposed to a single 532 nm Nd:YAG pulse, and normalized against an etched sample with no laser exposure. Since the XPS measurement was taken at an extreme angle of incidence, it was assumed that the spectrum would not reliably represent benchmark surface composition models. Each data point is an independent sample.

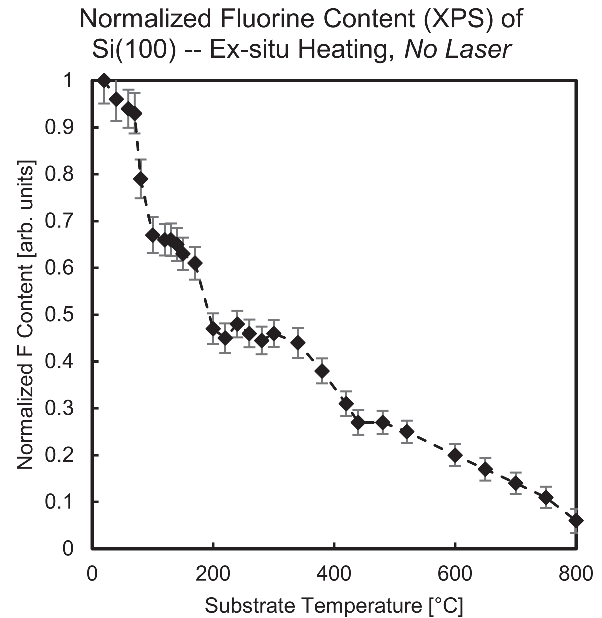


FIG. 8. Glancing angle XPS (75°) fluorine surface composition, for Si(100) etched with low ion energy Ar/$SF_6$ plasma and then heated *in-situ* in the XPS device to the specified temperature. All data are from one sample from which XPS spectra were obtained as the temperature was increased.

With the maximum Nd:YAG pulse rate of 100 Hz being a limiting factor, testing at much lower pressures (0.1, 0.2, and 1.0 mTorr) was carried out with varying pulse rates at a constant pulse energy of 40 mJ/cm$^2$.

For an $SF_6$/Ar recipe of 50:4 sccm, the depth removed per pulse was constant even at 100 Hz, as seen in Fig. 10. However, once the pressure was decreased to 0.2 mTorr, the material removed per pulse began dropping off at 50 Hz and 0.1 mTorr showed dropoff at 25 Hz. These timescales coincide with the estimated F surface saturation times with radical pressures on the order of the total pressure (marked in Fig. 10 with vertical lines of corresponding color for each pressure), which are easily calculated or determined by

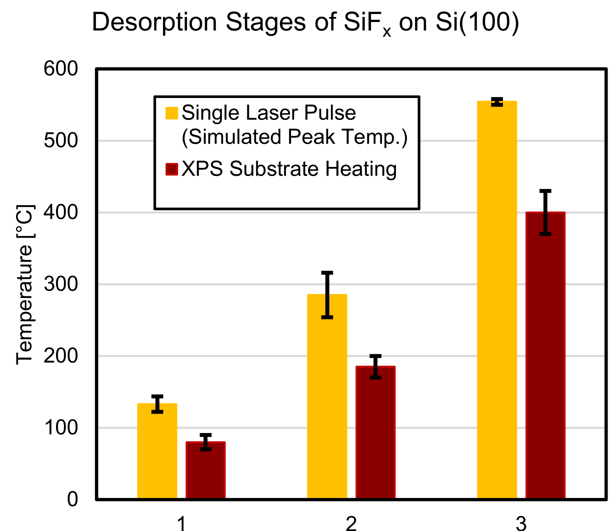


FIG. 9. Temperatures where $SiF_x$ desorption stages occurred, which manifest as significant drops in F surface coverage. Desorption due to substrate heating had much lower values for these thresholds compared to its laser-exposed counterpart.

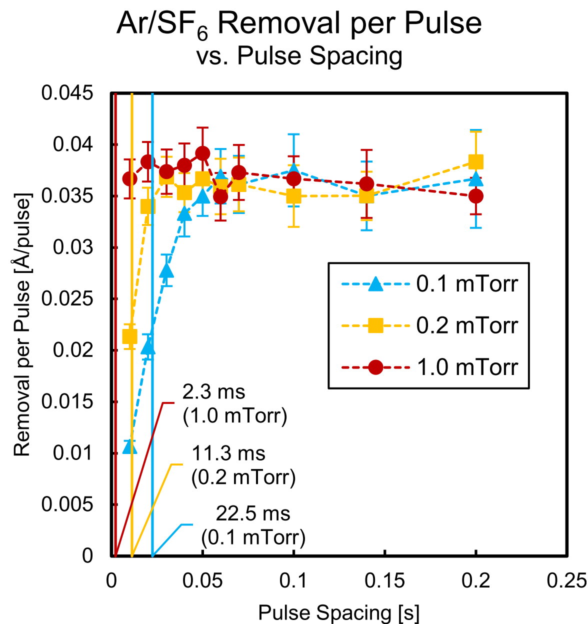


FIG. 10. Si material removal per pulse vs. Nd:YAG pulse spacing at 40 mJ/$cm^2$ at 532 nm. 1 ML fluorine surface coverage time is marked using vertical lines for 0.1, 0.2, and 1.0 mTorr (22.5, 11.3, and 2.3 ms, respectively) using their corresponding plot colors. Each data point is from a separate sample.

iconic plots such as those found in the study by Wolf and Tauber.[24]

Upon shifting to an $Ar/C_4F_8/O_2$ recipe of 50:8:1.5 sccm, the dropoff at short pulse spacing is still seen in Fig. 11. However, having too infrequent laser pulsing results in another dropoff, which is displayed in the right side of the graph. This additional effect, not seen in the $Ar/SF_6$ recipe, is due to the minimum laser power required to break through the $CF_x$ polymer layer, with an intermediate peak due to these two competing effects overlapping. With lower pressure, the polymer deposition rate is lower, and thus, the per-pulse removal peaks at lower and lower pulse rates.

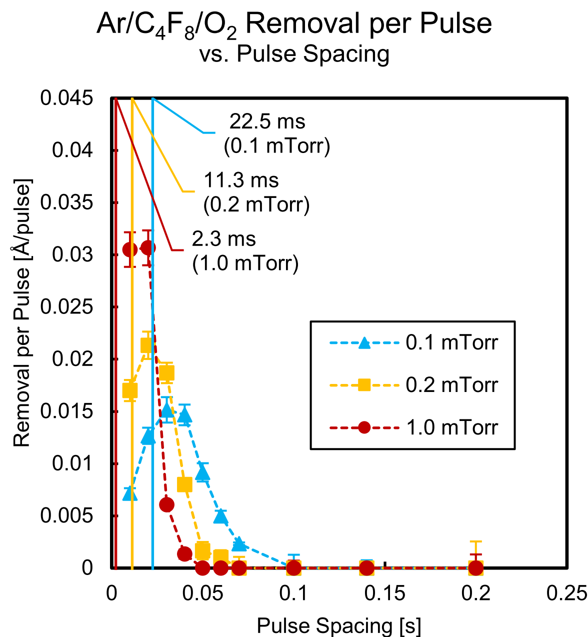


FIG. 11. Si material removal per Nd:YAG pulse vs. pulse-pulse spacing at 40 mJ/$cm^2$ at 532 nm in 20:4:1 sccm $Ar/C_4F_8/O_2$. More-infrequent laser pulses cause the net etch rate to fall to zero due to polymer deposition, while faster pulses (smaller pulse spacing) still show the diminishing return when faster than the surface saturation time. Lower pressures of 0.1, 0.2, and 1.0 mTorr, like Fig. 10, have their corresponding surface saturation times marked by the vertical line of the same color (22.5, 11.3, and 2.3 ms, respectively). Each data point is from a separate sample.

These tests confirmed that the laser-assisted etch process has mass transport limitations based on the surface saturation time for higher laser pulse rates, coinciding with the running model of desorption of involatile etch products. For both direct F etching in $SF_6$ and inhibitor etching in $C_4F_8$, the proper choice of pulse rate can help to utilize the full laser intensity and prevent wasted heat in the processed sample, alongside increasing throughput for a given laser output. An etching recipe at 10 mTorr, for example, can benefit from a pulse rate up to 4.4 kHz before diminishing returns are seen.

## IV. CONCLUSIONS

By coupling pulsed, high-intensity but low-average-power laser exposure with typical etch plasmas, a room temperature process was developed which could selectively etch Si over dielectrics through the optical selectivity of the laser line. Doping tests at constant wavelength, alongside glancing angle XPS data, showed that the etching mechanism by 532 nm light was through desorption of involatile etch products via thermal heating. Gas arrival tests through varying pulse rates and radical pressures showed that optimal per-pulse material removal by the laser without waste heat was achieved when pulse spacing remained below the projected time for the surface to saturate with etch radicals.

Etch rate enhancement depended on the absorption depth of the wavelength in the material, the pulse rate, and the density of etch radicals, with the increase of 2 Å/s at 30 mJ/$cm^2$/pulse (532 nm, 100 Hz) in Si being shown in this work. The scalability of this technique to full-wafer processing may be possible due to the low average power required although the cost and system incorporation are chief concerns. However, this process in lieu of RIE is highly compatible with restrictions of low thermal budget and low surface damage, which will make it attractive for manufacturing future generations of integrated circuits. A companion paper shows low-damage etching results with this technique.[25]


## ACKNOWLEDGMENTS

This work was conducted at the Center for Plasma-Material Interactions with material and professional support provided as a gift from Lam Research, Inc. Surface characterization techniques were primarily provided by the Frederick Seitz Materials Research Lab at the University of Illinois Urbana-Champaign.



[1]G. Moore, Electronics **38**, 8 (1965).
[2]D. N. Ruzic and J. R. Sporre, "Method of selective etching a three-dimensional structure," U.S. patent 9,171,733 B2 (27 October 2015).
[3]H. Shin, W. Zhu, V. M. Donnelly, and D. J. Economou, J. Vac. Sci. Technol. A **30**, 021306 (2012).
[4]C. Arnone and G. B. Scelsi, Appl. Phys. Lett. **54**, 225 (1989).
[5]W. Sesselmann, E. Hudeczek, and F. Bachmann, J. Vac. Sci. Technol. B **7**, 1284 (1989).

[6]J. L. Peyre, C. Vannier, D. Riviere, and G. Villela, Appl. Surf. Sci. **36**, 313–321 (1989).
[7]G. L. Loper, S. H. Suck-Salk, and M. D. Tabat, Appl. Surf. Sci. **36**, 257 (1989).
[8]D. Riedel, J. L. Hernandez-Pozos, and R. E. Palmer, Appl. Phys. A **78**, 381 (2004).
[9]C. H. Choy and K. W. Cheah, Appl. Phys. A **61**, 45 (1995).
[10]A. Kiani, K. Venkatakrishnan, B. Tan, and V. Venkataramanan, Opt. Express **19**, 10834 (2011).
[11]W. Holber, G. Reksten, and R. M. Osgood, Jr., Appl. Phys. Lett. **46**, 201 (1985).
[12]P. Leerungnawarat, H. Cho, S. J. Pearton, C.-M. N. Zetterling, and M. Ostling, J. Electron. Mater. **29**, 342 (2000).
[13]P. A. Maki and D. J. Ehrlich, Appl. Phys. Lett. **55**, 91 (1989).
[14]M. Ishii, T. Meguro, K. Gamo, T. Sugano, and Y. Aoyagi, Jpn. J. Appl. Phys., Part 1 **32**, 6178 (1993).
[15]N. Li, T. Yoshinobu, and H. Iwasaki, Jpn. J. Appl. Phys., Part 2 **37**, L995 (1998).
[16]S. J. Randolph, J. D. Fowlkes, and P. D. Rack, J. Appl. Phys. **98**, 034902 (2005).
[17]M. A. Lieberman and A. J. Lichtenberg, *Principles of Plasma Discharges and Materials Processing* (Wiley-Interscience, Hoboken, NJ, 2005), p. 546.
[18]J. A. Peck, "Laser-enhanced plasma etching of semiconductor materials," Ph.D. thesis (Department of Nuclear, Plasma and Radiological Engineering, University of Illinois at Urbana-Champaign, 2017), May 4.
[19]G. E. Jellison, Jr., F. A. Modine, C. W. White, and R. F. Wood, Phys. Rev. Lett. **46**, 1414 (1981).
[20]Y.-R. Luo, *Comprehensive Handbook of Chemical Bond Energies* (CRC Press, Boca Raton, FL, 2007).
[21]S.-P. Jeng and T.-P. Ma, Appl. Phys. Lett. **61**, 1310 (1992).
[22]D. P. Pullman, A. A. Tsekouras, Y. L. Li, J. J. Yang, M. R. Tate, D. B. Gosalvez, K. B. Laughlin, M. T. Schulberg, and S. T. Ceyer, J. Phys. Chem. B **105**, 486 (2001).
[23]S. Tinck, E. C. Neyts, and A. Bogaerts, J. Phys. Chem. C **118**, 30315 (2014).
[24]S. Wolf and R. N. Tauber, *Silicon Processing for the VLSI Era* (Lattice Press, Sunset Beach, CA, 1986).
[25]J. A. Peck and D. N. Ruzic, "Sub-damage-threshold plasma etching and profile tailoring of Si through laser-stimulated thermal desorption," J. Vac. Sci. Technol. A (to be published).